Effects of axonal time delay on synchronization and wave formation in sparsely coupled neuronal oscillators

Tae-Wook Ko* and G. Bard Ermentrout†
Department of Mathematics, University of Pittsburgh, Pennsylvania 15260, USA
(Received 1 March 2007; revised manuscript received 29 June 2007; published 8 November 2007)

We investigate the effects of axonal time delay when the neuronal oscillators are coupled by sparse and random connections. Using phase-reduced models with general coupling functions, we show that a small fraction of connections with time delay can destabilize synchronous states and induce near-regular wave states. An order parameter is introduced to characterize those states. We analyze the systems using mean-field-type approximation.

DOI: 10.1103/PhysRevE.76.056206 PACS number(s): 89.75.Kd, 87.19.La, 02.30.Ks, 05.45.Xt

I. INTRODUCTION

Populations of coupled oscillators have been investigated as models of many physical, chemical, and biological systems [1–5]. In many cases, the oscillators are distributed spatially and, in such systems, waves and synchrony are of particular interest. Especially in neuroscience, these two phenomena have been observed and considered in relation with the information processing and abnormal brain functioning [4–7]. In distributed oscillator systems, the range of connections and the connection topology structure affect the dynamics of the systems. It has been argued that long-range coupling helps the synchronization of neuronal systems [7]. The recent introduction of the concept of small-world network [8] has strengthened these kinds of ideas. From the point of view of the Watts-Strogatz small-world network, neurons of the brain are coupled mainly locally but also connected through sparse long-range connections. Without costing much for the wiring of the brain, the system can achieve synchronization by reducing the average path length between neurons through the sparse long-range coupling [7,9].

On the other hand, it has been shown that desynchronizing long-range coupling can destabilize the synchronous states and induce other states. The prototypical mechanism is the so-called Mexican-hat-type connection: short-range synchronizing and long-range desynchronizing connections [10]. In Ref. [11], the behavior of chains of oscillators with local synchronizing coupling and long-range desynchronizing coupling between end points and points in the middle was studied. The system was shown to exhibit various types of waves. This system is a good example showing that sparse long-range coupling can economically, in the sense of wiring cost, desynchronize the system and induce regular waves.

One way to produce desynchronization at long ranges is to introduce distance-dependent delays. Time-delayed coupling can be desynchronizing or synchronizing depending on the type of the coupling and the magnitude of the time delay. States due to the desynchronizing effects of time delay have been reported [12–22] along with synchronous states: antiphase states in two coupled oscillators [12], disorganized states in a two-dimensional array of oscillators coupled to nearest neighbors with uniform time delay [13], and incoherent states in all-to-all coupled oscillators with uniform time delay [14–16]. The authors of Refs. [17–21] reported that time delays can induce waves with long-range coupling. In Ref. [17], using the phase-reduction method, the authors showed that axonal time delay which was modeled as proportional to the distance between oscillators can destabilize the synchronous states and cause the formation of waves in an infinite line. They showed that a large space constant for the decay of synaptic coupling and a low conduction velocity result in a loss of synchrony. Space-dependent delays due to the axodendritic interactions in an array of integrate-and-fire neurons with dendritic structure were also shown to have similar effects on the stability of synchronous states and generation of traveling waves [18,19]. Similar results with distance-dependent time delays were reported in all-to-all coupled oscillators on a ring [20] and a two-dimensional array of long-range coupled oscillators [21]. The effects of distance-dependent delays on propagation of wave fronts were also studied in the firing rate models [23,24]. However, these studies were done with the regular connection structures between oscillators. In reality, including neural systems, coupling topologies are not generally regular [7–9]. These studies need to be extended to the case of complex coupling topologies. Recently, it was shown in Ref. [22] for the case with an idealized coupling function that distance-dependent time delay can induce near in-phase synchronous states or near-regular waves when the oscillators are sparsely randomly connected.

In this paper, in the same context of Ref. [22] but with general coupling functions, we investigate the effects of axonal time delay when the neuronal oscillators are connected by sparse and random connections. We find that even a small fraction of connections with time delay can destabilize synchronous states and induce near-regular wave states. A new useful order parameter is introduced to quantify the regularity of the states. Using a mean-field-type approximation, we can analyze the states and find the stability condition of the states. The "sparseness" is economic in the viewpoint of wiring cost and sufficient to provide desynchronizing effect.

II. MODEL AND NUMERICAL SIMULATIONS

We use phase models in our simulations and analysis. The phase-reduction method has been used to study the dynamics

*taewook@pitt.edu
†bard@math.pitt.edu

of coupled oscillators, because it greatly reduces the complexity of the system and describes behaviors such as synchrony and waves clearly [1–5,25–27]. For any system of weakly coupled nearly identical limit-cycle oscillators, the system can be reduced to a phase-only system where each oscillator is represented by a single scalar phase and the interaction is given by the sum of pairwise interactions depending only on the phase difference of the interacting oscillators [1–5,25–27].

The phase-reduction approach also has the advantage that delays in the interactions become phase shifts in the coupling function when the time delay is comparable with one or a few periods of an oscillation [26–28]. In cases, where time delays are the same for all the coupling, the system can be regarded as a system with a different coupling function in the absence of time delays and can be understood in the same frame as phase reduction without time delay [4]. However, when time delays are not the same due to the reasons such as the inhomogeneity of the speed of signal processing or signal propagation, and the inhomogeneity of the distance over which the signal propagates, the system cannot be considered in that way. Instead, such system may show richer behavior.

In this study, we consider the case of sparsely coupled identical neurons on a ring, where the axonal conduction is slow enough to cause a time delay that can be approximately modeled as the time required for the signal propagate distance between the oscillators with a constant speed. We also assume that the maximum time delay is comparable with one or a few periods of an isolated oscillator. The phase model for this system can be written as follows:

$$\dot{\theta}_i(t) = \omega + \frac{K}{\bar{n}} \sum_{j=1}^{N} A_{ij} H\left(\theta_j(t) - \theta_i(t) - \frac{2\pi}{T} \frac{r_{ij}}{v} \right), \quad i = 1,2, \ldots, N, \tag{1}$$

where $\theta_i(t)$ is the phase of the ith oscillator at time t, ω is the natural frequency of oscillators, and N is the total number of oscillators. The oscillators are located on a ring with circumference L. Note that in contrast to the cases of no time delay or uniform time delay, the positions of oscillators are important in the cases with distance-dependent time delay. Here, we consider the case of equal spacing between oscillators, in which oscillator i is located at $x_i = i\Delta x = \frac{L}{N} i$ measured counterclockwise relative to a certain reference point on the ring. The main results do not change with the mild irregularity of the spacing. r_{ij} is the distance which is unambiguously given by the shorter Euclidean distance between oscillators i and j *along* the ring, $r_{ij} = \min\{|x_j - x_i|, L - |x_j - x_i|\}$. The term "distance" should not be confused with the "path length" defined along the network in network theory (see, e.g., Ref. [8]).

The second term on the right-hand side of Eq. (1) denotes the coupling between oscillator i and other oscillators. Oscillator i is coupled to n_i oscillators with coupling strength K according to a coupling topology described by an adjacency matrix A. $\bar{n}$ is the average number of neighbors which are directly connected to an oscillator. Assuming bidirectional interaction between oscillators, we take the element of adjacency matrix $A_{ij} = A_{ji} = 1$, if two oscillators i and j interact, and $A_{ij} = A_{ji} = 0$ otherwise.

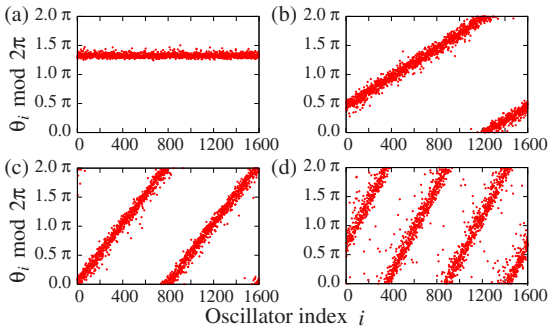

FIG. 1. (Color online) Phase of the oscillators along the ring for different time delays. (a) $\tau' = 0.3$, (b) 0.9, (c) 1.8, and (d) 3.5. $H(\theta) = \sin(\theta)$. $\omega = \pi/2$, $N = 1600$, $L = 1$, $\tau' \equiv L\tau$, $K = 1.0$, and $\bar{n} = 40$ ($p = 0.025$). (a) $\tau' = 0.3$, a near-synchronous state (winding number $m = 0$, $R_0 \approx 0.995$, $R_{m\neq 0} < 0.01$), $\Omega_{\mathrm{av}} \approx 1.137$, and $\sigma_\Omega < 10^{-5}$. (b) $\tau' = 0.9$, a wave state $m = 1$ ($R_1 \approx 0.979$, $R_{m\neq 1} < 0.02$), $\Omega_{\mathrm{av}} \approx 1.635$, and $\sigma_\Omega < 10^{-5}$. (c) $\tau' = 1.8$, a wave state $m = 2$ ($R_2 \approx 0.968$, $R_{m\neq 2} < 0.02$), $\Omega_{\mathrm{av}} \approx 1.696$, and σ_Ω oscillates irregularly in [0.002 53, 0.007 13]. (d) $\tau' = 3.5$, a wave state $m = 3$ ($R_3 \approx 0.89$, $R_{m\neq 3} < 0.03$), Ω_{av} oscillates irregularly in [1.295, 1.305], and σ_Ω oscillates irregularly in [0.057, 0.078].

In the coupling term, H is the coupling function obtained by the phase-reduction method for pairwise interactions [4,5]. H is a 2π periodic function and, in the absence of time delays, depends only on the phase difference of the interacting oscillators. It was shown that time delay causes negative phase shift $\xi = -\frac{2\pi\eta}{T}$, where η is the delay and T is the period [26–28]. The coupling between oscillators i and j is assumed to be mediated by a signal propagating the distance r_{ij} between the oscillators with constant speed v. The finite speed of signal causes the time delay r_{ij}/v. Thus, we have phase shift $-\frac{2\pi}{T}\frac{r_{ij}}{v}$.

To remove the complication due to the representation of distance, we treat the index in Eq. (1) as N periodic such that index $i \pm N$ is equivalent to i and rewrite Eq. (1) as

$$\dot{\theta}_i = \omega + \frac{K}{\bar{n}} \sum_{l=-N/2}^{N/2-1} A_{i,i+l} H(\theta_{i+l} - \theta_i - 2\pi\tau|l|\Delta x), \quad i = 1,2, \ldots, N, \tag{2}$$

where $\theta_i = \theta_i(t)$ and τ is the ratio of unit time delay to the period of the oscillator, $\tau \equiv \frac{1/v}{T}$. Let us call τ the relative unit time delay. Note that it is not the absolute value of $1/v$ or T but the ratio τ that determines the dynamics.

Figure 1 shows the phases of oscillators along the ring in numerical simulations of Eq. (2) with $H(\theta) = \sin(\theta)$. In this paper, we simulate the system using fourth-order Runge-Kutta method with time step $\Delta t = 0.01$. We use initial conditions of several types (i) $\theta_i(0)$ chosen randomly from $[-\pi, \pi]$ (uniformly incoherent) or (ii) $\theta_i(0) = 2\pi i m/N + \epsilon_i$, where m is an integer and ϵ_i is a random number chosen from $(-\delta, \delta)$ with δ small. From now on, the connection topology discussed in this paper is random. In Fig. 1, the total number of oscillators $N = 1600$ and the average number of neighbors $\bar{n} = 40$ (equivalently, the connection probability

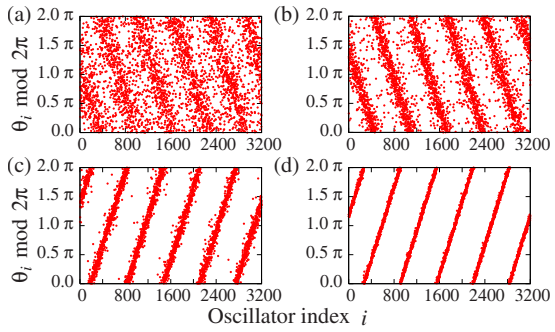

FIG. 2. (Color online) Phase of the oscillators along the ring for different average number of neighbors (a) $\bar{n}=15$, (b) 20, (c) 40, and (d) 80. $H(\theta)=H_{\text{crook}}(\theta)$ [29]. $\omega=\pi/2$, $N=3200$, $L=1$, $\tau'\equiv L\tau=4.64$, and $K=1.0$. (a) $\bar{n}=15$ ($p=0.004\ 6875$), R_{-5} and R_5 oscillate irregularly in [0.005, 0.42] and [0.005, 0.395], respectively. The state changes irregularly between the high R_{-5} state and the high R_5 state. R_{-5} and R_5 move in an anticorrelated manner, $R_{m\neq\pm5}<0.045$. Ω_{av} oscillates irregularly in [3.842, 3.908] and σ_Ω oscillates irregularly in [0.465, 0.602]. (b) $\bar{n}=20$ ($p=0.006\ 25$), a wave state with winding number $m=-5$. R_{-5} oscillates irregularly in [0.682, 0.725] and $R_{m\neq-5}<0.025$. Ω_{av} oscillates irregularly in [3.785, 3.82] and σ_Ω oscillates irregularly in [0.237, 0.303]. (c) $\bar{n}=40$ ($p=0.0125$), a wave state with $m=5$, $R_5\approx0.94$, $R_{m\neq5}<0.012$. Ω_{av} oscillates irregularly in [3.643, 3.648] and σ_Ω oscillates irregularly in [0.02, 0.09]. (d) $\bar{n}=80$ ($p=0.025$), a wave state with $m=5$, $R_5\approx0.993$, $R_{m\neq5}<0.006$, $\Omega_{\text{av}}\approx3.558$, and $\sigma_\Omega<10^{-5}$.

$p=0.025$). Even though each oscillator is connected to only a small fraction of the whole population, the system exhibits near-synchronous states and wave states, depending on the time delays. This result is essentially the same as those reported in Ref. [22]. Simulations with the $H(\theta)$ function obtained from a model for a real neuronal coupling [17,29] show similar behaviors (see Fig. 2).

To quantify the oscillating behaviors of the system in the simulation, we measure the average frequency $\Omega_{\text{av}}(t)$ over the whole oscillators and the dispersion $\sigma_\Omega(t)$ of the frequency distribution [22],

$$\Omega_{\text{av}}(t) \equiv \langle \dot{\theta}(t) \rangle \equiv \frac{1}{N}\sum_{i}^{N} \dot{\theta}_i(t), \tag{3}$$

$$\sigma_\Omega(t) \equiv \sqrt{\langle [\dot{\theta}(t)-\Omega_{\text{av}}(t)]^2 \rangle} = \sqrt{\frac{1}{N}\sum_{i}^{N} [\dot{\theta}_i(t)-\Omega_{\text{av}}(t)]^2}. \tag{4}$$

The smallness of the dispersion $\sigma_\Omega(t)$ of a state reflects that the state approaches a frequency synchronized state where all the oscillators oscillate with the same frequency $\Omega_{\text{av}}(t)$. For a given set of parameters, especially, ω and K which determine the time scale of the system, the states in Figs. 1(a)–1(d) have relatively small dispersion σ_Ω, and thus we can say that the system exhibits nearly frequency synchronized oscillations.

We also introduce an order parameter generalized from Kuramoto's order parameter [1,2] to measure how close a state is to a perfect synchronous state or to a perfect wave state,

$$R_m \equiv \frac{1}{N}\left| \sum_{i=1}^{N} \exp\left[i\left(\theta_i - \frac{2\pi m x_i}{L} \right) \right] \right|, \tag{5}$$

where m is the winding number of a reference state to which we measure the resemblance of the state. With $m=0$, this order parameter is reduced to that of Kuramoto. The phase difference, $\theta_i-\frac{2\pi m x_i}{L}$, denotes the phase deviation from a perfect phase distribution. For a perfect synchronous state or for a perfect wave state with winding number m_0, R_{m_0} is one since the phase difference with $m=m_0$ is the same for all i. In contrast, R_m is zero for $m\neq m_0$. For states which are not perfect, R_m gives values according to the resemblance to the perfect ones. R_m is a measure of the regularity of states. Based on the order parameter values, we can tell which category a given state belongs to. R_m values calculated for the states in Fig. 1 reflect the states well as described. For the well-defined states, such as those in Fig. 1, the fluctuation of the time series of R_m is small and R_m approaches a stationary value.

To see the effect of the average number of neighbors or the connection probability, we simulate with different conditions for fixed time delay. Figure 2 shows the simulation results with different average number $\bar{n}$ of neighbors. As expected, the state looks more like that of all-to-all coupling for increased $\bar{n}$. But transition from disorganized incoherent state to the organized wave state occurs with relatively small connection probability. In Fig. 3, we calculate R_m values for the states obtained with various $\bar{n}$ for several different N values. Figure 3(a) shows the results with different time delays. The time delays are chosen according to the stability analysis discussed in the next section to guarantee the stability of the states. Even though the transition point to an ordered state shifts depending on the time delay, it occurs at a relatively small $\bar{n}$ compared to the total number of oscillators. Figure 3(b) shows the dependence of R_m on $\bar{n}$ for different N values. The dependence is qualitatively the same for different N values. The transition to the ordered states occurs at the similar $\bar{n}$ which corresponds to a smaller wiring probability p for a larger system. This implies that $\bar{n}$ rather than p determines the dynamics. With the similarity between random coupling and simple random sampling of statistics [30], this observation is consistent with the fact that, in simple random sampling, the size of the sample representing a large population is nearly independent of the size of the population [30]. In neural systems, we can expect that the numbers of connections are sufficient to cause desynchronization and regular wave formation, even though the connections are very sparse [9].

III. MEAN-FIELD-TYPE ANALYSIS

Now let us analyze the system using an approximate equation. In the limit of $N\to\infty$ and $n_i\to\infty$ for all i, the summation term $\Sigma A_{i,i+l}H(\cdot)$ of Eq. (2) could be approximated by

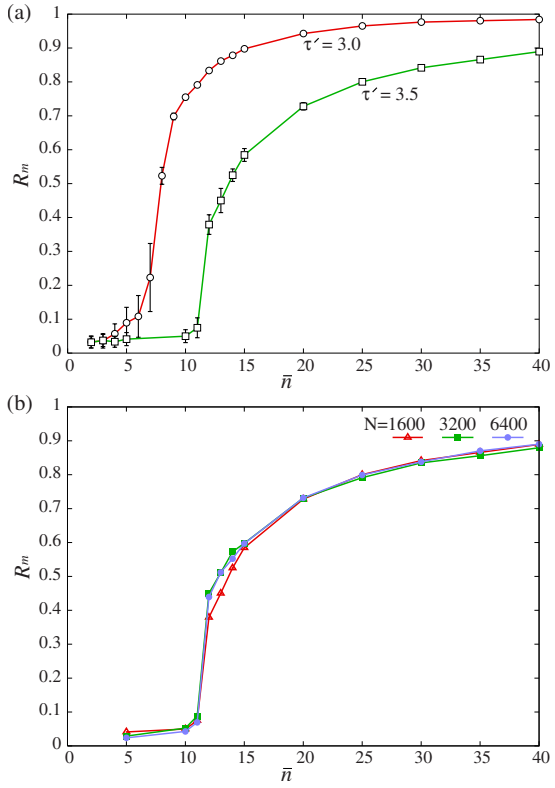

FIG. 3. (Color online) Typical trend of order parameter R_m as a function of the average number $\bar{n}$ of neighbors. $H(\theta)=\sin(\theta)$ and system parameters are the same as Fig. 1 except N, $\bar{n}$, and τ'. (a) R_m for the states with $\tau'=3.0$ and $\tau'=3.5$. $N=1600$. We compute both $R_{m=3}$ and $R_{m=-3}$ for each state obtained from simulations, and denote the larger one. The symbols represent the time average of R_m and the error bars denote the standard deviation of R_m time series. The curves are guides for the eyes. (b) R_m for the states with $N=1600$, 3200, and 6400 for $\tau'=3.5$. Error bars with similar sizes for each data point as in (a) are omitted for the simplicity of the figure.

$\Sigma P_{i,i+l}H(\cdot)$, where $P_{i,i+l}$ is the probability of connection between oscillator i and $i+l$. In other words, $P_{i,j}$ is the probability of finding connection between the oscillators in the ensemble of the networks and the weighted sum $\Sigma_l P_{i,i+l}H(\cdot)$ is the ensemble average of the sum $\Sigma_l A_{i,i+l}H(\cdot)$. So the sum $\Sigma_l P_{i,i+l}H(\cdot)$ gives a good approximate value of $\Sigma_l A_{i,i+l}H(\cdot)$ when both N and n_i are large enough. As Fig. 3(b) shows, this approximation is good even for very sparsely coupled cases with $n_i \ll N$ as long as n_i is large enough. In addition to this approximation, if we take the limit of $\Delta x \to 0$, we can convert the approximate equation for discrete oscillators into an equation for a continuum of oscillators,

$$\frac{\partial\theta(x,t)}{\partial t} = \omega + \frac{K}{\bar{n}\Delta x}\left(\int_{-L/2}^{L/2} P(x,x+y)H(\theta(x+y,t)-\theta(x,t) - 2\pi\tau|y|)dy\right), \tag{6}$$

where $P(x,y)$ is the probability of connection between oscillator at position x and y, and the average connection is given by $\bar{n}=\frac{1}{L\Delta x}\int_{-L/2}^{L/2}\int_{-L/2}^{L/2}P(x,y)dydx$. Scaling the variables and the parameters by $x'=x/L$, $y'=y/L$, and $\tau'=L\tau$, we can get an N- and L-independent equation,

$$\frac{\partial\hat{\theta}(x',t)}{\partial t} = \omega + \frac{K}{\bar{P}}\left(\int_{-1/2}^{1/2}\hat{P}(x',x'+y')H(\hat{\theta}(x'+y',t)-\hat{\theta}(x',t) - 2\pi\tau'|y'|)dy'\right), \tag{7}$$

where $\bar{P}$ is the average connecting probability given by $\bar{P}=\int_{-1/2}^{1/2}\int_{-1/2}^{1/2}\hat{P}(x',y')dy'dx'$, $\hat{\theta}(x',t)\equiv\theta(Lx',t)$, and $\hat{P}(x',x'+y')\equiv P(Lx',Lx'+Ly')$. To simplify the notation, without loss of generality, we assume that $L=1$. Now we can ignore $\hat{}$ over θ and P.

When $P(x,x+y)$ is independent of x and depends only on y, the system is translationally invariant and thus can have exact synchronous solutions or wave solutions. This is the case for our randomly coupled oscillators.

For the random network case of this study, the connection probability $P(x,x+y)$ is a constant. Equation (7) for $P(x,x+y)=p$, a constant, becomes

$$\frac{\partial\theta(x',t)}{\partial t} = \omega + K\int_{-1/2}^{1/2}H(\theta(x'+y',t)-\theta(x',t) - 2\pi\tau'|y'|)dy'. \tag{8}$$

Note that Eq. (8) is exactly the same form as that of the all-to-all coupling case. We can expect similar behaviors observed with regular long-range coupling [17]. There is no p in Eq. (8), because we normalize the coupling term by the mean number of neighbors. This normalization does not affect the stability of the system because the oscillators are identical, but it affects frequencies of the oscillators. So the sparsely coupled oscillators can have similar phase distribution with all-to-all coupled cases regardless of the normalization. However, if the coupling terms in both of the cases are divided by the same constant instead of the mean number of neighbors, the coupling term is proportional to p and the sparsely coupled oscillators move slowly toward the phase distribution with a speed proportional to p.

To identify the possible solutions, let us assume the solutions of the form

$$\theta(x',t) = \Omega_k t + kx', \quad k = 2m\pi, \quad m = 0, \pm 1, \pm 2, \ldots, \tag{9}$$

where Ω_k, k, and m are the synchronization frequency, the wave vector, and the winding number, respectively. Because of symmetry, the behavior with $-m$ and m is identical, so we restrict the analysis to $m \geq 0$. Substituting $\theta(x',t)$ in Eq. (9) into Eq. (8), we obtain

$$\Omega_k = \omega + K\int_{-1/2}^{1/2}H(ky'-2\pi\tau'|y'|)dy' = \omega + K\left(\int_0^{1/2}H(ky' - 2\pi\tau'y')dy' + \int_{-1/2}^{0}H(ky'+2\pi\tau'y')dy'\right). \tag{10}$$

Figure 4(a) shows the synchronization frequency Ω as a

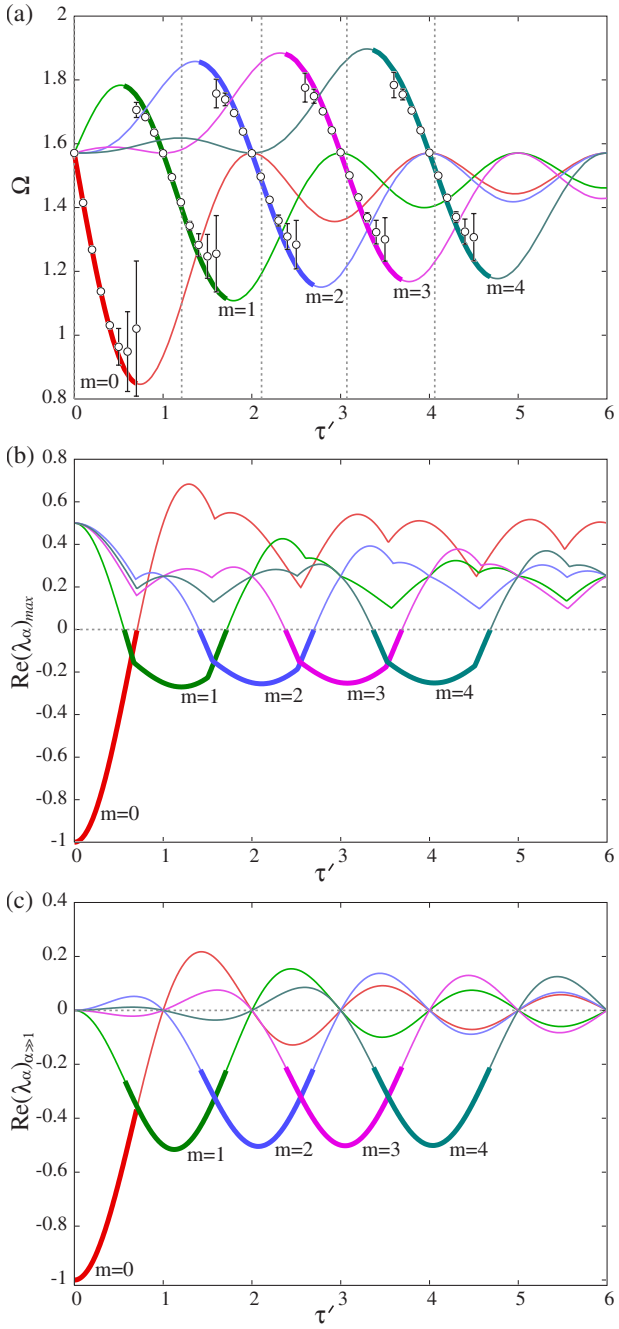

FIG. 4. (Color online) States and their stability as a function of scaled relative time delay $\tau'=L\tau$ for the case with $H(\theta)=\sin(\theta)$, $\omega=\pi/2$, and $K=1$. Thick parts of the curves in (a), (b), and (c) correspond to the stable states identified by linear stability analysis of Eq. (8). (a) Synchronization frequency Ω. m is the winding number of a state. Curves are obtained from Eq. (10). Symbols and error bars denote the time average of $\Omega_{\mathrm{av}}(t)$ and $\sigma_\Omega(t)$ defined by Eq. (4), respectively. Simulations are carried out with $N=1600$ and $\bar{n}=40$ ($p=0.025$). Dashed vertical lines denote τ' values with which $\mathrm{Re}(\lambda_\alpha)_{\max}$ of (b) has minimum values. (b) The maximum real part of eigenvalue λ_α. $\mathrm{Re}(\lambda_\alpha)$ is given by Eq. (14). $\mathrm{Re}(\lambda_\alpha)_{\max}<0$ is the condition for the linear stability. (c) $\mathrm{Re}(\lambda_\alpha)$ for perturbations with large wave vector $\alpha\gg 1$. $\mathrm{Re}(\lambda_\alpha)_{\alpha\gg 1}$ is given by Eq. (15) and $\mathrm{Re}(\lambda_\alpha)_{a\gg 1}<0$ is a necessary condition for the stability of corresponding states.

function of scaled relative unit time delay τ' and winding number m for a coupling function $H(\theta)=\sin(\theta)$ and a fixed coupling strength $K=1$. The curves for synchronization frequency Ω are obtained from Eq. (10) and the synchronization frequencies denoted by symbols are obtained from numerical simulations of randomly coupled oscillators. The thick parts of the curves denote the stable region obtained by the linear analysis of Eq. (8). The stability of the states are discussed later in this section. Each curve for m fits well with the simulation results for the τ' values around the τ'_0 value for which the corresponding curve in Fig. 4(b) for the stability has minimum negative value, and thus, the state can be said to be most stable. The deviation from the predicted values is larger as τ' moves away from τ'_0. Error bars in Fig. 4(a) denote the time average of the dispersion $\sigma_\Omega(t)$ of oscillating frequencies. The dispersions also have similar trend. They are small around the most stable states and become larger as the state moves far from the most stable ones. Figure 3(a) also reflects this trend. As the average number of neighbors $\bar{n}$ decreases, the order parameter for $\tau'=3.0$ deep inside the stability region shows slower decrease from one than that for $\tau'=3.5$ near the boundary of the region. Because of this trend, we see that as $\bar{n}$ decreases, the states near the boundary of the stability regions start to deviate more from the perfect states and parameter regions agreeing well with the perfect state shrinking toward the most stable states. So the regions which can be identified as bistable regions also shrink and disappear in Fig. 4(a) as we decrease $\bar{n}$. But, as Fig. 3(b) for $\tau'=3.5$ near the boundary of the stability region shows, we can get highly ordered states for parameters near the boundary of the stability regions for sparse networks as long as $\bar{n}$ is large enough and thus can see the bistability regions for sparse networks with finite but large $\bar{n}$. Figure 5(a) is a similar figure with coupling function $H(\theta)$ obtained from a model for a real neuron [17,29]. Details of the figure including the existence of bistable regions depend on the coupling functions.

There is a possibility of states other than synchronous states or wave states being stable in the stability regions or outside of the regions. But, we obtain only synchronous states or wave states for the conditions inside the stability regions from numerical simulations with our random initial conditions. This shows that if other states are stable in the stability regions, they may have small sizes of basin of attraction or cannot be reached from such random initial conditions. Outside of the stability regions as in Fig. 5 and regions near the boundary of the stability regions, we obtain states distorted from perfect states. The distortion is due to the oscillators which come to have frequencies significantly different from others. Typically, such oscillator groups are not fixed and change over time. For all-to-all coupling cases, we observe continuous variation of frequency over space, but, for randomly coupled cases, the frequency shows discontinuous variation over space and the deviating oscillators are often spatially localized. The distorted states look similar to those states of the adjacent stability regions and can have high order parameters. As we see similar distorted states in all-to-all coupling cases, the order parameter does not asymptote at 1 with increasing $\bar{n}$ outside of the stability regions and this tells us that these distorted states are not mainly due

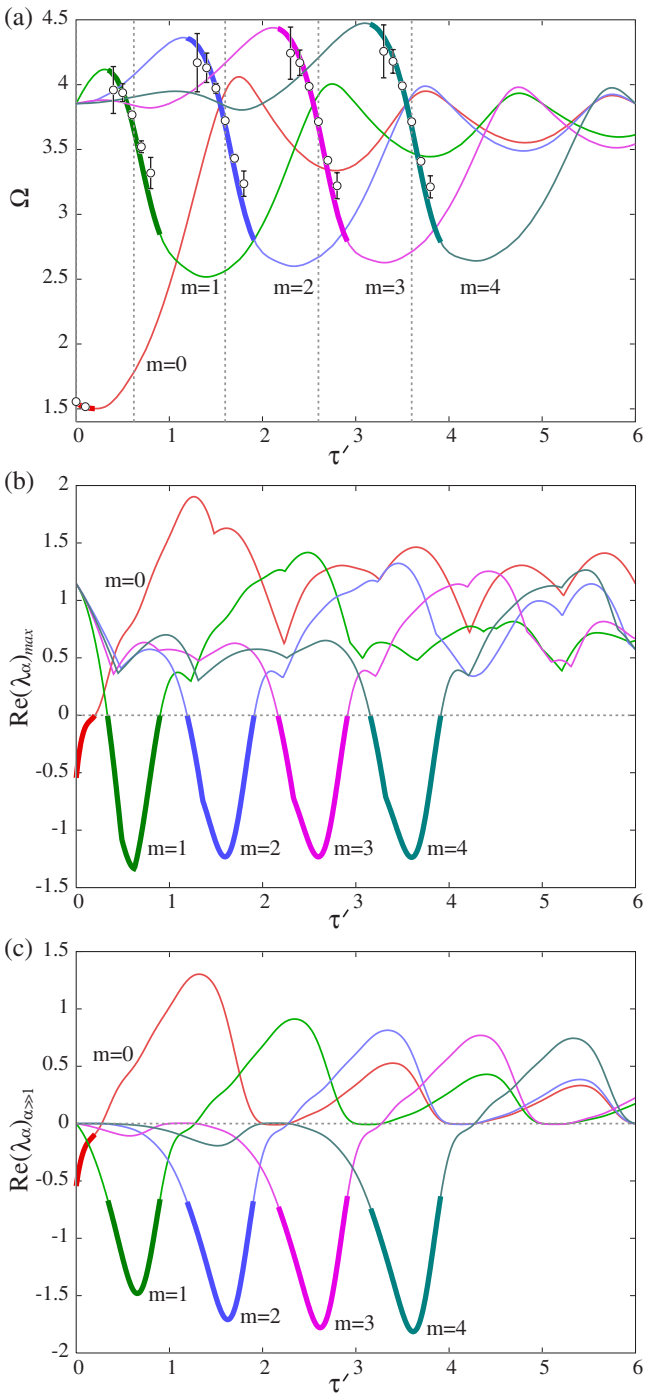

FIG. 5. (Color online) States and their stability as a function of scaled relative time delay $\tau' = L\tau$ for the case with $H(\theta) = H_{\text{crook}}(\theta)$ [29], $\omega = \pi/2$, and $K = 1$. (a) Synchronization frequency Ω. Simulations are carried out with $N = 1600$ and $\bar{n} = 80$ ($p = 0.05$). (b) The maximum real part of the eigenvalue λ_α. (c) $\text{Re}(\lambda_\alpha)$ for perturbations with large wave vector $\alpha \gg 1$. For other details, refer to the caption of Fig. 4.

to the finite $\bar{n}$ but due to the instabilities from the frequency locked states. The frequency dispersion $\sigma_\Omega(t)$ of the distorted states is large and the average frequency $\Omega_{av}(t)$ deviates significantly from the frequency of Eq. (10) obtained for perfect states, as is expected. This is also true for the case with all-to-all coupling.

We notice that the curves of Figs. 4(a) and 5(a) have similar shapes for large m and/or τ' in each case. We can understand this observation as follows. In general, a 2π-periodic coupling function $H(\theta)$ can be written as a Fourier series,

$$H(\theta) = c_0 + \sum_{n=1} c_n \sin(n\theta + \beta_n), \quad c_n \geq 0. \tag{11}$$

With the second term of $H(\theta)$ in Eq. (11), the second integral of Eq. (10) gives the summations of terms like $\frac{-c_n \cos(n(k+2\pi\tau')y' + \beta_n)}{n(k+2\pi\tau')}$ evaluated over a given range. For a large k or τ, this value is order of $(k+2\pi\tau')^{-1}$, and thus can be ignored compared to the first integral with the same term. In those cases, Ω_k can be approximated as the following:

$$\Omega_k \approx \omega + K\left(c_0 + \int_0^{1/2} H_1(ky' - 2\pi\tau' y')dy'\right), \tag{12}$$

where $H_1(\theta) = H(\theta) - c_0$. Ω_k has a shape which is conserved under the transformations $k \to k + 2s\pi$ and $\tau' \to \tau' + s$ for an integer s. This is the property manifested in Figs. 4(a) and 5(a). Curves for different k values have similar shape shifted by integer τ' values for large k and/or τ'. This holds for general $H(\theta)$.

Let us consider the stability of the solutions. To determine the stability of the solutions, we linearize Eq. (7) around the solution Eq. (9) by letting $\theta(x',t) = \Omega_k t + kx' + \epsilon\phi(x',t)$ with $\epsilon \ll 1$,

$$\frac{\partial\phi(x',t)}{\partial t} = K\left(\int_{-1/2}^{1/2} H'(ky' - 2\pi\tau'|y'|)(\phi(x'+y',t) - \phi(x',t))dy'\right), \tag{13}$$

where H' indicates the derivative of the function with respect to its argument. The solutions of Eq. (13) have the form $\phi(x,t) = e^{i\alpha x}e^{\lambda_\alpha t}$, where α has the form $2\pi q$ with $q = 0, \pm 1, \pm 2, \ldots$. Thus, formal stability for the approximate system, Eq. (7), is assured if the real part of λ_α is negative for all possible α. Inserting this into Eq. (13) and taking the real part of λ_α which determines the stability, we get

$$\text{Re}(\lambda_\alpha) = K\int_{-1/2}^{1/2} H'(ky' - 2\pi\tau'|y'|)[\cos(\alpha y') - 1]dy'. \tag{14}$$

For fixed parameters, we numerically calculate $\text{Re}(\lambda_\alpha)$ as we change α and find the maximum values $\text{Re}(\lambda_\alpha)_{\max}$ as a function of τ'. Figures 4(b) and 5(b) show $\text{Re}(\lambda_\alpha)_{\max}$. We can rephrase the stability condition: when the value $\text{Re}(\lambda_\alpha)_{\max}$ is negative, the corresponding state is stable. In Figs. 4 and 5, we denote the stability region as thick curves. The end points of the thick curves correspond to the bifurcation points. Simulation results with sparse random coupling fit well with the stability region obtained. For corresponding all-to-all coupling cases, the condition defines the exact stable region

for perfect synchronous states and wave state.

Finding simple conditions from Eq. (14) for a general coupling function is not easy. Instead, we can find a simple necessary condition for the stability. For a solution to be stable, $\mathrm{Re}(\lambda_\alpha)$ should be negative for all possible α. Therefore, a necessary condition for the stability is the condition $\mathrm{Re}(\lambda_\alpha)<0$ for $\alpha \gg 1$. Inserting $H(\theta)$ in the form of Eq. (11) into Eq. (14), we can see that the integral of $H'(ky' - 2\pi\tau'|y'|)\cos(\alpha y')$ is order of α^{-1} and vanishes for large α.

Thus, the necessary condition for the stability of the solutions is

$$\begin{aligned}\mathrm{Re}(\lambda_\alpha)_{\alpha\gg 1} &\approx -K\int_{-1/2}^{1/2} H'(ky' - 2\pi\tau'|y'|)dy' \\ &= -\frac{K}{k-2\pi\tau'}\left[H\left(\frac{1}{2}(k-2\pi\tau')\right) - H(0)\right] \\ &\quad + \frac{K}{k+2\pi\tau'}\left[H\left(-\frac{1}{2}(k+2\pi\tau')\right) - H(0)\right] < 0.\end{aligned} \tag{15}$$

Figures 4(c) and 5(c) show the validity of the necessary condition for each case. Only the states satisfying the necessary condition $\mathrm{Re}(\lambda_\alpha)_{\alpha\gg 1}<0$ can be stable.

IV. SUMMARY AND DISCUSSION

In this paper, using phase-reduced models with general coupling functions, we have shown that axonal time delay, which can be distance dependent, can destabilize the synchronous state and/or induce waves in sparsely connected neural systems. There are several ways to produce waves in systems of oscillators [5]: (i) local pacemakers, (ii) frequency gradients, (iii) coupling anisotropy, and (iv) pattern formation. The present paper concerns the latter mechanism. The role of delays here is to destabilize the synchronous state due to the long-distance desynchronizing of the "effective" coupling function (phase shifted due to the delays). In other words, we can say that Mexican-hat-type mechanism, short-range synchronizing and long-range desynchronizing, occurs effectively by time delays in this system [10,17]. In the absence of distance-dependent delays, sparse long-range coupling encourages synchrony, but when there is a "penalty" to pay for this (for example, delays in getting information there), synchrony can actually be destabilized with the result, the emergence of traveling waves as the only stable attractor. The noticeable thing is that sparse long-range coupling can efficiently induce regular waves without costing much for the wiring of the system. In this sense, even though neurons in neural systems are sparsely coupled in complicated ways [9], the connection seems to be enough to make time delay cause desynchronization and possibly wave formation. Related to this study, it would be interesting to see the effect of random sparse long-range desynchronizing inhibitory coupling on wave formation in the systems with local synchronizing coupling [31].

The authors were supported by National Science Foundation Grant No. DMS05135.

[1] Y. Kuramoto,*Chemical Oscillations, Waves, and Turbulence* (Springer, Berlin, 1984); S. H. Strogatz, Physica D **143**, 1 (2000).
[2] J. A. Acebrón *et al.*, Rev. Mod. Phys. **77**, 137 (2005).
[3] A. T. Winfree, *The Geometry of Biological Time*, 2nd ed. (Springer-Verlag, New York, 2001).
[4] P. Tass, *Phase Resetting in Medicine and Biology* (Springer, Berlin, 1999).
[5] G. B. Ermentrout and D. Kleinfeld, Neuron **29**, 33 (2001).
[6] D. Rubino, K. A. Robbins, and N. G. Hatsopoulos, Nat. Neurosci. **9**, 1549 (2006).
[7] G. Buzsáki, *Rhythms of the Brain* (Oxford University Press, New York, 2006).
[8] S. H. Strogatz, Nature (London) **410**, 268 (2001).
[9] S. B. Laughlin and T. J. Sejnowski, Science **301**, 1870 (2003).
[10] J. D. Murray, *Mathematical Biology* (Springer, Berlin, 1989).
[11] G. B. Ermentrout and N. Kopell, SIAM J. Appl. Math. **54**, 478 (1994).
[12] H. G. Schuster and P. Wagner, Prog. Theor. Phys. **81**, 939 (1989).
[13] E. Niebur, H. G. Schuster, and D. M. Kammen, Phys. Rev. Lett. **67**, 2753 (1991).
[14] S. Kim, S. H. Park, and C. S. Ryu, Phys. Rev. Lett. **79**, 2911 (1997).
[15] M. K. S. Yeung and S. H. Strogatz, Phys. Rev. Lett. **82**, 648 (1999).
[16] M. Y. Choi, H. J. Kim, D. Kim, and H. Hong, Phys. Rev. E **61**, 371 (2000).
[17] S. M. Crook, G. B. Ermentrout, M. C. Vanier, and J. M. Bower, J. Comput. Neurosci. **4**, 161 (1997).
[18] P. C. Bressloff and S. Coombes, Phys. Rev. Lett. **78**, 4665 (1997).
[19] P. C. Bressloff and S. Coombes, Int. J. Mod. Phys. B **11**, 2343 (1997).
[20] D. H. Zanette, Phys. Rev. E **62**, 3167 (2000).
[21] S.-O. Jeong, T.-W. Ko, and H.-T. Moon, Phys. Rev. Lett. **89**, 154104 (2002).
[22] T.-W. Ko, S.-O. Jeong, and H.-T. Moon, Phys. Rev. E **69**, 056106 (2004).
[23] M. A. P. Idiart and L. F. Abbott, Network **4**, 285 (1993).
[24] S. Coombes, G. J. Lord, and M. R. Owen, Physica D **178**, 219 (2003).
[25] G. B. Ermentrout and N. Kopell, J. Math. Biol. **29**, 195 (1991).
[26] G. B. Ermentrout, in *Neural Modeling and Neural Networks*, edited by F. Ventriglia (Pergamon, Oxford, 1994), p. 79.
[27] F. C. Hoppensteadt and E. M. Izhikevich, *Weakly Connected Neural Networks* (Springer-Verlag, New York, 1997).

[28] E. M. Izhikevich, Phys. Rev. E **58**, 905 (1998).
[29] Here, $H_{\text{crook}}(\theta)$ is a coupling function from a model for a real neuronal coupling [17]: $H_{\text{crook}}(\theta)=2.283\ 14-1.5457\ \cos(\theta)-0.738\ 241\ \cos(2\theta)-0.092\ 9315\ \cos(3\theta)+0.034\ 5372\ \cos(4\theta)+0.044\ 0749\ \cos(5\theta)+2.289\ 48\ \sin(\theta)-0.248\ 993\ \sin(2\theta)-0.228\ 386\ \sin(3\theta)-0.096\ 1023\ \sin(4\theta)-0.035\ 3857\ \sin(5\theta)$.
[30] S. K. Thompson, *Sampling*, 2nd ed. (Wiley, New York, 2002).
[31] F. G. Kazanci and G. B. Ermentrout, SIAM J. Appl. Math. **67**, 512 (2007).